Solid State Phenomena
ISSN: 1662-9779, Vol. 390, pp 173-180
doi:10.4028/p-aiq9fM

Submitted: 2026-01-19
Revised: 2026-02-18
Accepted: 2026-02-20
Online: 2026-04-17

Investigation of Friction Coefficient at Stack Compression Tests

Martin László Kölüs[1,3,a*], Imre Nagy-Gombai[2,b], Gábor Kalácska[1,c] and Gábor Jozsef Beres[3,d]

[1]Institute of Technology, Hungarian University of Agriculture and Life Sciences (MATE), 2100 Gödöllő, Páter blvd. 1. Hungary

[2]ElringKlinger Hungary Ltd., 6000 Kecskemét, Paul Lechler St. 4, Hungary

[3]Mechanical- and Laser Beam Technologies Research Group, John von Neumann University, 6000 Kecskemét, Izsáki St. 10. Hungary

[a*]kolus.martin@nje.hu, [b]Imre.Nagy-Gombai@elringklinger.com, [c]kalacska.gabor@uni-mate.hu, [d]beres.gabor@nje.hu

*Corresponding author

Keywords: stack compression test, friction, finite element method.

Abstract. During sheet metal forming (for example, deep drawing), the desired geometry is typically produced under large plastic deformations. However, in order to characterize the material behavior in this deformation range as accurately as possible, experimental investigation of the material is indispensable. Such investigations are necessary, among other reasons, to determine material properties that may later serve as input parameters for finite element (FEM) simulations. By defining appropriate material properties, the design and optimization of the forming technology become more efficient. One such property is the material's flow curve; for determining it in the large deformation range, a particularly promising method is the stack compression test (SCT). At the same time, the method also has certain drawbacks. One is that the test is not standardized, and therefore there is no exact methodology for its execution. Another difficulty arises from the fact that the friction conditions present during the test are not clearly defined. This paper seeks to determine whether the friction conditions in the case of the SCT can be inferred by a comparative analysis of experimental force–displacement curves and force–displacement curves obtained from FEM simulations.

Introduction

One of the most widely known methods for determining a flow curve is the tensile test–based approach; however, this method is not capable of achieving the level of deformation that is characteristic of more complex sheet metal forming processes. To overcome this limitation, alternative procedures such as the plane strain compression test (PSCT), applied by Neag and Balan [1], and the hydraulic bulge test (HBT) used by Coppieters et al. (2020) [2], have been developed. In their work, Coppieters et al. (2022) [3] provide a comprehensive overview of the available experimental methods for determining flow curves in the large deformation regime. They also refer to the stack compression method, which was among the first to be applied by Merklein and Kuppert [4].

Subsequently, An and Vegter [5] investigated the influence of hydrostatic pressure and frictional behavior during the execution of the SCT. Kuwabara et al. [6] also presented a comprehensive study on the effect of hydrostatic pressure on the flow stress, commonly referred to as the strength differential effect. Their results indicated that the applied lubricant may deteriorate as a consequence of oil film thinning and elongation during deformation. Furthermore, Kraus et al. [7] suggested treating the friction coefficient as a variable rather than a constant parameter, experimentally determining the evolution of both the Coulomb friction coefficient and the friction factor. The pressure-dependent variation of these frictional parameters was subsequently described mathematically by Gil et al. [8], who employed a nonlinear formulation to characterize the evolution of lubrication conditions.

Finite element method (FEM) simulations are frequently used for tool geometry optimization, as demonstrated by R. LU et al. [9]. In their study, they also investigated the stress and strain distributions arising during the deep drawing of Ti/Al bimetal sheets. Wang et al. [10] examined the prediction of ductile fracture occurring during sheet metal forming using finite element methods and subsequently validated their results experimentally. In the present work, we aim to obtain a more accurate understanding of the frictional conditions prevailing during the SCT by comparing experimental results with FEM simulation outcomes.

Used Material

For the experiment, DC04 (EN 10130 EU) cold-rolled thin steel sheet was used, which owing to its ferritic microstructure, has favorable formability properties and is therefore widely applied across many areas of industry for the manufacture of components produced by complex deep-drawing operations. The chemical composition of the base material is presented in Table 1.

Table 1. Average chemical composition (percentage) of the DC04 steel.

C [%]	Mn [%]	P [%]	S [%]	Si [%]	Al [%]	N [%]
0.0355	0.239	0.0135	0.0088	0.0177	0.0471	0.0097

The mechanical properties and anisotropy characteristics of the material were determined by means of a standard tensile test (ISO 6892-1:2019) at room temperature using an INSTRON 4482 universal testing machine. The strength and plasticity properties were examined in the rolling direction, perpendicular to it, and at 45°. The results are presented in Table 2.

Table 2. The average material parameters of the DC04 steel.

YS [N/mm^2]	UTS [N/mm^2]	A_{80} [%]	A_g [%]	r_0 [-]	r_{45} [-]	r_{90} [-]	$\bar{r}$ [-]
229	336	37.9	20.4	1.823	1.311	2.380	1.706

Where *YS* is yield strength; *UTS* is ultimate tensile strength; *A80* is total elongation; *Ag* is uniform elongation and the *r* values are the anisotropy parameters.

Preparation and Execution of the Stack Compression Test

The stack compression tests, similarly to the previously mentioned material characterizations, were also carried out using the INSTRON testing machine. In accordance with our previous work [11], a machine compliance correction was applied. Cylindrical tool platens with polished pressing surfaces, manufactured from Böhler K110 (X153CrMoV12), were used in the experiments. The heat treatment of the tool platens was performed based on the manufacturer's recommendations. Proper positioning of the specimens both on top of each other and on the compression dies is also crucial; therefore, a positioning device manufactured additively from PLA material was used. The compression dies and the positioning device are shown in Fig. 1.

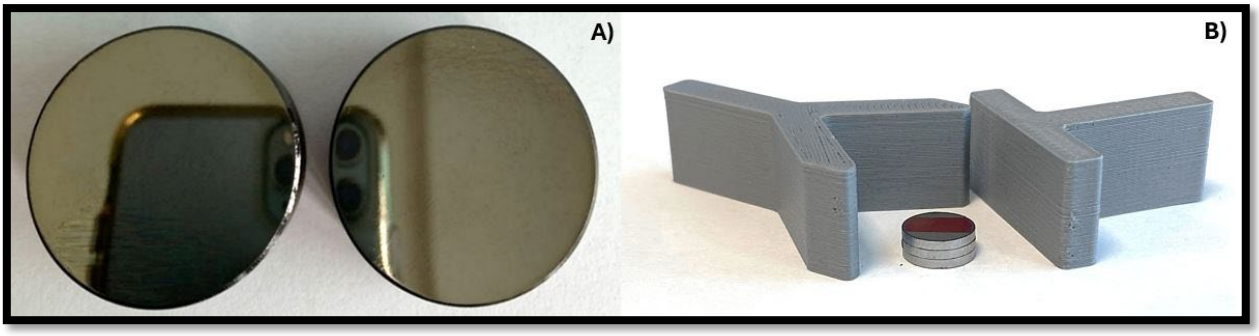

Fig. 1. The polished compression dies A) and the positioning device B).

From the base material with a thickness of 1 mm, cylindrical specimens were manufactured by laser cutting. One set of specimens had an initial diameter of 6 mm, while the other set had an initial diameter of 10 mm. The stacks were assembled such that their height was half of the initial diameter *(h/d = 1/2)*; therefore, in the first case a test configuration of Ø6 × h3 mm was used, while in the second case a Ø10 × h5 mm configuration was applied.

The surfaces of the compression platens in contact with the specimens were coated with Luba 21® high-pressure lubricant in order to minimize friction. In contrast, the surfaces of the specimens in contact with each other were not lubricated, thereby promoting bulk-like material behavior. The specimens were placed at the center of the compression tool so that the rolling direction markers (red markings) shown in part B) of Figure 1 faced the same direction. The tests were terminated when the compressed height of the stack approximately reached half of the initial height. The initial test configuration and the compressed stacks are illustrated in Fig. 2.

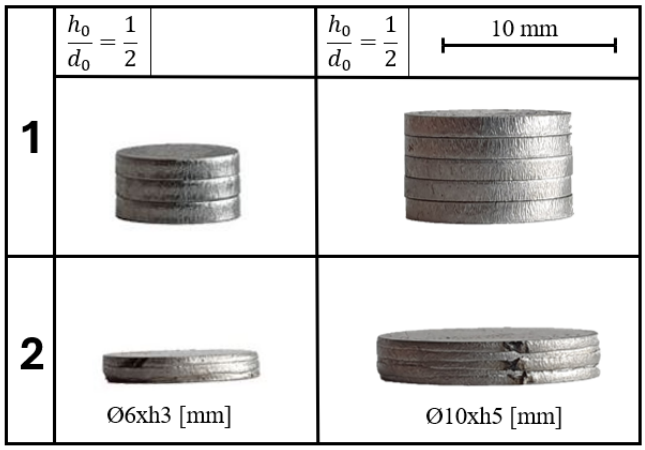

Fig. 2. The experimental setups before (1) and after the SCT (2).

Compression began with a rapid approach (v_{rapid} = 3 [mm/min]) up to a load of 250 [N], after which it continued according to the following relation: h/10 [mm/min]. This procedure was necessary to ensure that, after the initial clamping phase, the same strain rate was maintained in both cases.

The Structure of the Simulations

The material properties of the workpieces were defined according to the values listed in Table 2. The applied flow curve was obtained from tensile test results previously performed by the authors.

The finite element simulations were carried out using Simufact Forming 2025.02, which is based on the nonlinear implicit solver MSC Marc. An incremental–iterative Newton–Raphson scheme was applied, accounting for geometric nonlinearity (large strain formulation), material nonlinearity (elasto-plastic behavior), and contact nonlinearity. In order to reduce the computational time, the model was reduced to a quarter. Accordingly, the appropriate symmetry boundary conditions were applied to the quarter-specimen.

Meshing of the specimens was performed using the sheetmesh option, which employs hexahedral elements and, as its name suggests, is specifically designed for meshing sheet metal components. For the simulation of the different experimental setups, the mesh element sizes were scaled proportionally to each other. The most important meshing parameters for both configurations are summarized in Table 3.

Table 3. The parameters of the meshes used.

Diameter [mm]	Elem size	Elements over thickness	Element count	Min. edge angle
6	0.1	3	2193	30°
10	0.16	3	2193	30°

The software does not allow the creation of more than one deformable specimen within a single simulation. Therefore, the stack configuration was realized by introducing additional tool elements whose material behavior was changed from rigid to deformable and assigning them identical material parameters to the original specimen. This modeling approach does not modify the boundary conditions or contact definitions and therefore does not influence the force–stroke response of the simulation. The mesh applied to the specimens is illustrated in Fig. 3.

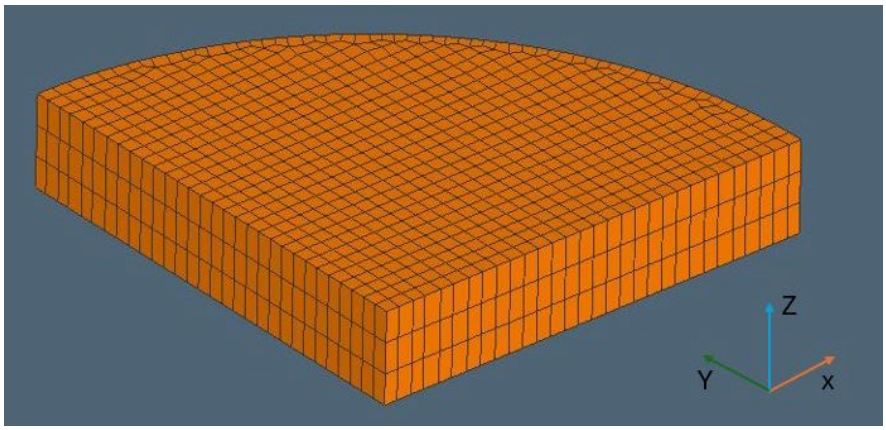

Fig. 3. The mesh applied to the specimens.

In Fig. 3, the X direction corresponds to the rolling direction of the material, Y denotes the transverse direction, and Z represents the thickness direction. Figure 4 illustrates the assembled FEM simulation of the Ø10 × h5 mm configuration.

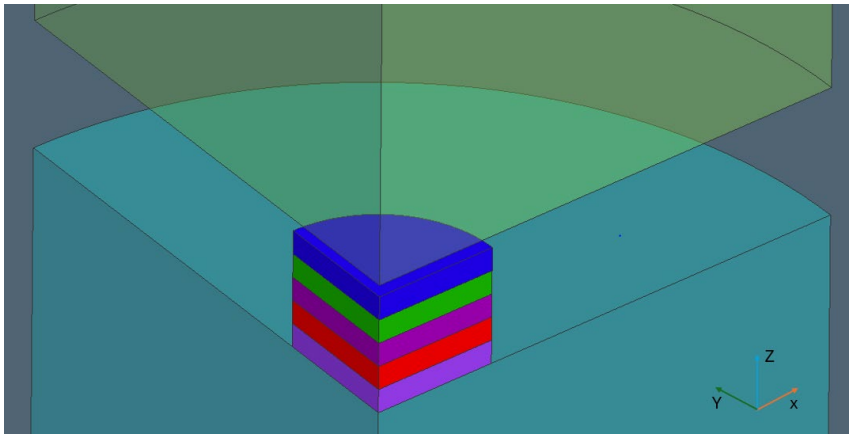

Fig. 4. The FEM simulation of the Ø10 × h5 mm experimental setup.

The temperature was also specified and set to 20 °C. In addition, a remeshing criterion was defined; in the present case, it was based on the angular distortion within individual elements, with an allowable limit of 15°. Furthermore, all specimens were compressed to half of their initial height, consistent with the experimental procedure, while maintaining the same deformation rate.

During the simulation, a Coulomb friction coefficient (μ) was applied and defined using two values. The first coefficient (μ_{die}) was assigned to the lubricated contact surfaces between the pressure plates and the workpieces, while the second coefficient ($\mu_{specimen}$) was applied to the contact surfaces between the workpieces themselves. The combinations of friction coefficients used in the process are summarized in Table 4.

Table 4. The Coulomb friction coefficient combinations used.

Cases	μ	1.	2.	3.	4.	5.
A	μ_{die}	*0.045*	*0.057*	*0.075*	*0.085*	*0.11*
	$\mu_{specimen}$	*0.4*	*0.4*	*0.4*	*0.4*	*0.4*
B	μ_{die}	*0.075*	*0.075*	*0.075*	-	-
	$\mu_{specimen}$	*0.2*	*0.3*	*0.4*	-	-

The final time step of the executed FEM simulations is shown in Fig. 5. The specimen is compressed to 1.5 mm, and the effective strain is shown on the color scale; however, the current study does not consider strain values.

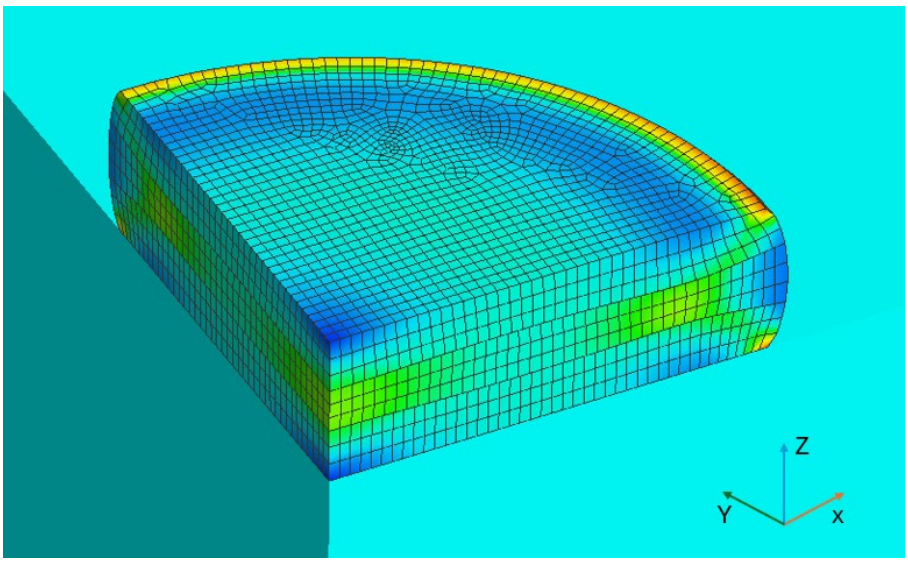

Fig. 5. The finished FEM simulation of the Ø6 × h3 mm experimental setup.

Comparison of Force–Stroke Curves Obtained from Experiment and FEM Simulations

From the simulations, it was possible to export the force–stroke diagrams of the compressed stacks corresponding to the individual friction coefficient combinations, which are then compared with the experimental measurement results. For each setup, the comparisons of the curves for cases A and B are presented separately. Fig. 6 and fig. 7 illustrates the curves for the Ø6 × h3 configuration in cases A and B.

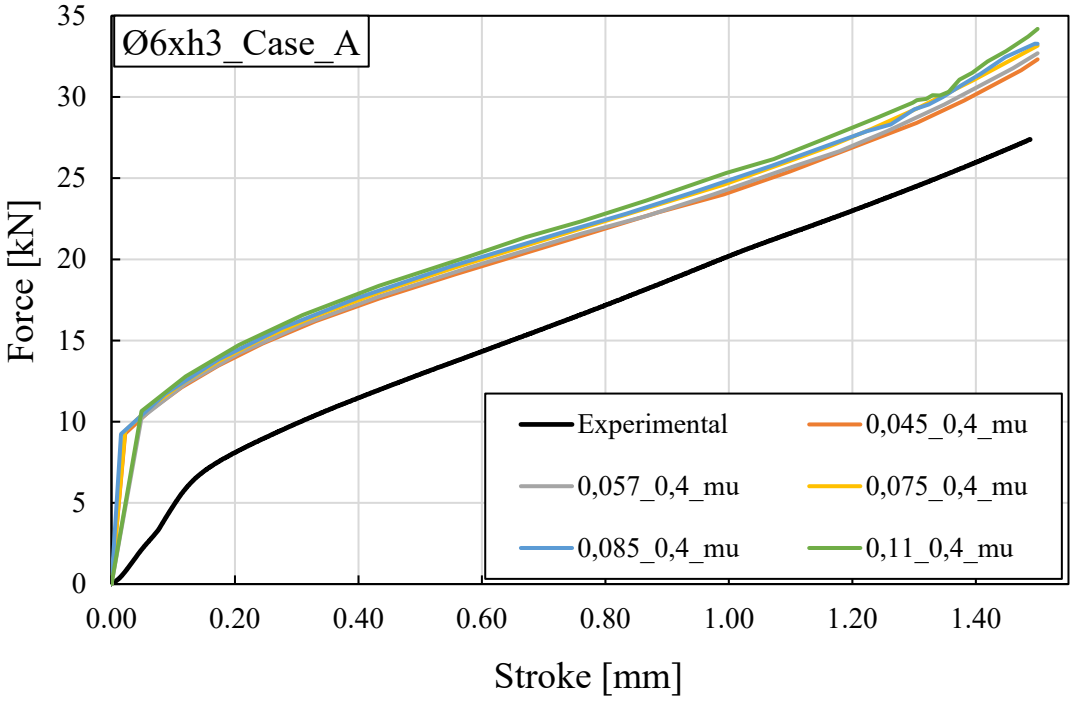

Fig. 6. The force-stroke curves for the Ø6 × h3 configuration in case A.

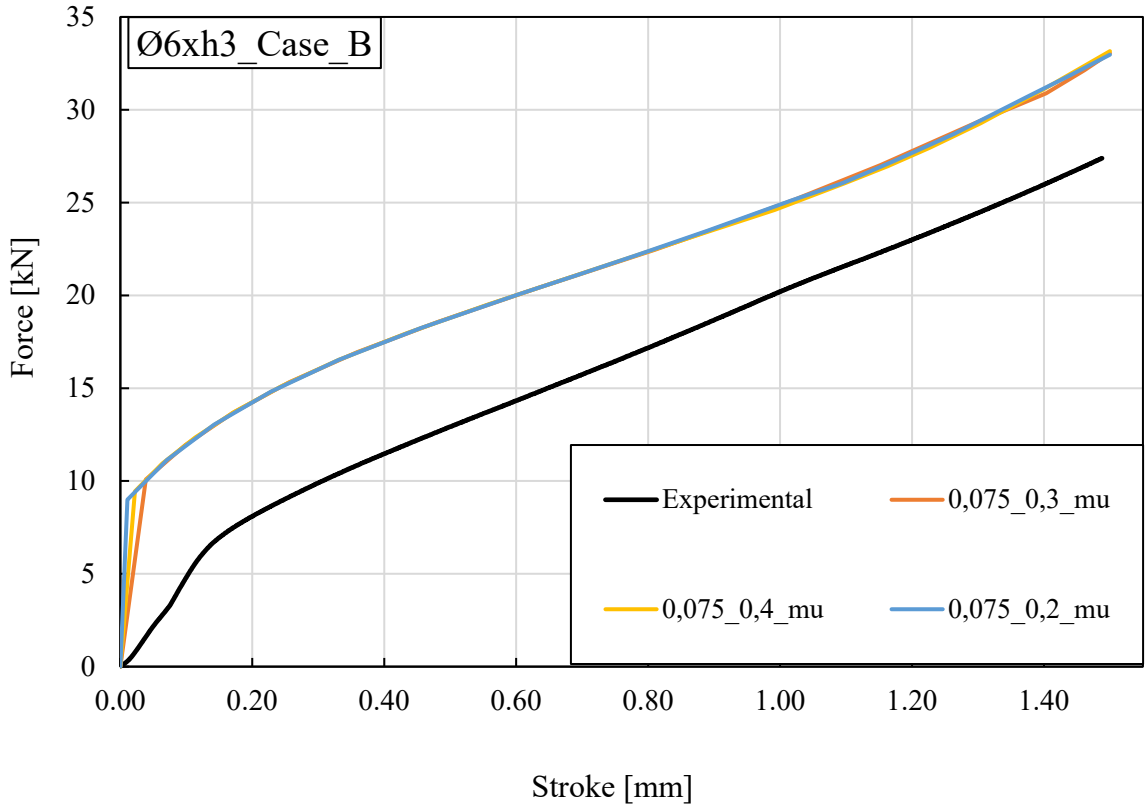

Fig. 7. The force-stroke curves for the Ø6 × h3 configuration in case B.

Fig. 8 and fig. 9 illustrates the curves for the Ø10 × h5 configuration in case A and B.

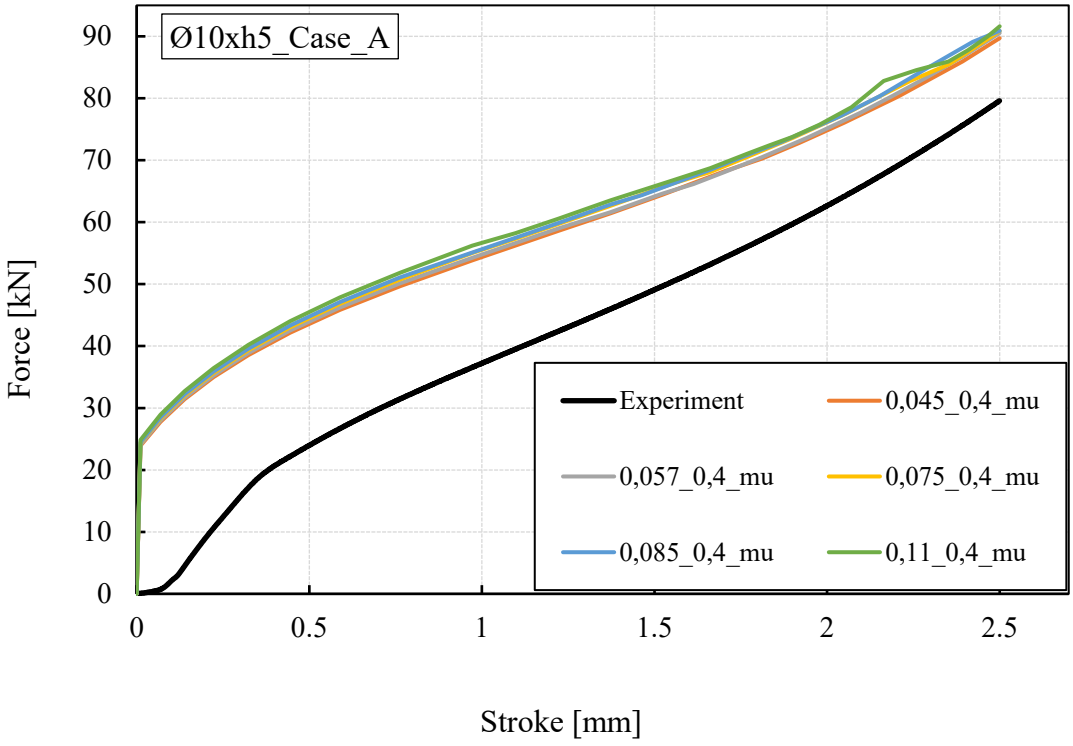

Fig. 8. The force-stroke curves for the Ø10 × h5 configuration in case A.

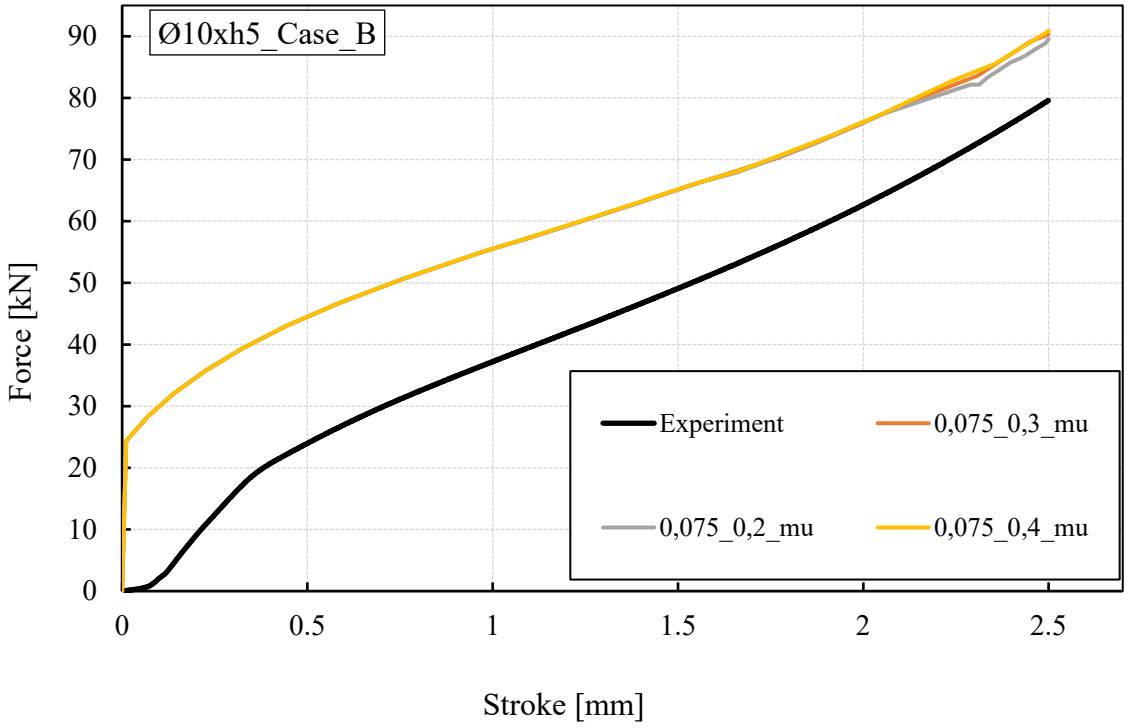

Fig. 9. The force-stroke curves for the Ø10 × h5 configuration in case B.

Summary

Our results indicate that, in terms of their overall characteristics, the measured and simulated force–stroke curves do not initially show good agreement; however, as the process progresses, a good correlation can be observed. Nevertheless, no common intersection point is present in any of the cases. The curves obtained from the FEM simulations predict higher forces than those measured experimentally. In the Ø6 × h3 configuration, this difference amounts to approximately 5–7 kN, whereas in the Ø10 × h5 case it is on the order of ~10 kN. It can be observed that, for the simulated curves, case A results in a larger difference in the magnitude of the maximum compressive force for both configurations. This difference is approximately 1.9 kN for both the Ø6 × h3 and Ø10 × h5 cases; however, it is proportionally more significant for the Ø6 × h3 configuration, where the maximum compressive force is only about 30 kN. For the simulated case B configuration, the observed difference is approximately 1.4 kN for the Ø10 × h5 case, while for the Ø6 × h3 configuration it is only about 0.2 kN. Based on these findings, it can be concluded that the friction coefficient between the compression dies and the workpieces likely has a greater influence on the process than the friction coefficient between the workpieces themselves.

Acknowledgement

Supported by the EKÖP-25 new national excellence program of the ministry for culture and innovation from the source of the national research, development and innovation fund.

References

[1] Neag A, Balan T. Verification of flow curve determination from plane strain compression tests. CIRP J Manuf Sci Technol 2025;63:554–65. https://doi.org/10.1016/j.cirpj.2025.11.005.

[2] Coppieters S, Jackel M, Kraus C, Kuwabara T, Barlat F. Influence of a Hydrostatic Pressure Shift on the Flow Stress in Sheet Metal. Procedia Manuf 2020;47:1245–9. https://doi.org/10.1016/J.PROMFG.2020.04.196.

[3] Coppieters S, Traphöner H, Stiebert F, Balan T, Kuwabara T, Tekkaya AE. Large strain flow curve identification for sheet metal. J Mater Process Technol 2022;308:117725. https://doi.org/10.1016/J.JMATPROTEC.2022.117725.

[4] Merklein M, Kuppert A. A method for the layer compression test considering the anisotropic material behavior. International Journal of Material Forming 2009;2:483–6. https://doi.org/10.1007/S12289-009-0592-8/METRICS.

[5] An YG, Vegter H. Analytical and experimental study of frictional behavior in through-thickness compression test. J Mater Process Technol 2005;160:148–55. https://doi.org/10.1016/j.jmatprotec.2004.05.026.

[6] Kuwabara T, Tachibana R, Takada Y, Koizumi T, Coppieters S, Barlat F. Effect of hydrostatic stress on the strength differential effect in low-carbon steel sheet. International Journal of Material Forming 2022;15:13. https://doi.org/10.1007/s12289-022-01650-2.

[7] Kraus M, Lenzen M, Merklein M. Contact pressure-dependent friction characterization by using a single sheet metal compression test. Wear 2021;476:203679. https://doi.org/10.1016/j.wear.2021.203679.

[8] Gil I, Mendiguren J, Galdos L, Mugarra E, Saenz de Argandoña E. Influence of the pressure dependent coefficient of friction on deep drawing springback predictions. Tribol Int 2016;103:266–73. https://doi.org/10.1016/J.TRIBOINT.2016.07.004.

[9] LU R, LIU Y, LI M, YAN M, SUN J, HUANG H. A pathway to refined stress and strain distributions in aerospace-grade Ti/Al bi-metal sheets: Synergizing theoretical insights and FEM simulations. Chinese Journal of Aeronautics 2024;37:493–516. https://doi.org/10.1016/j.cja.2024.07.025.

[10] Wang C, Daniel WJT, Lu H, Liu S, Meehan PA. FEM Investigation of Ductile Fracture Prediction in Two-Point Incremental Sheet Metal Forming process. Procedia Eng 2017;207:836–41. https://doi.org/10.1016/j.proeng.2017.10.838.

[11] KÖLÜS ML, BORBÉLY Richárd, BÉRES Gábor J. The effect of friction compensation on the slope of flow curves obtained by stack compression tests, 2024, p. 1182–9. https://doi.org/10.21741/9781644903131-131.